Depdc5 knockout rat: A novel model of mTORopathy

Elise Marsan, Saeko Ishida, Adrien Schramm, Sarah Weckhuysen, Giuseppe Muraca, Sarah Lecas, Ning Liang, Caroline Treins, Mario Pende, Delphine Roussel, et al.

Neurobiology of Disease 89 (2016) 180–189

Contents lists available at ScienceDirect

Neurobiology of Disease

journal homepage: www.elsevier.com/locate/ynbdi

Depdc5 knockout rat: A novel model of mTORopathy

Elise Marsan [a,b,c,d,1], Saeko Ishida [a,b,c,d,1], Adrien Schramm [a,b,c,d], Sarah Weckhuysen [a,b,c,d], Giuseppe Muraca [a,b,c,d], Sarah Lecas [a,b,c,d], Ning Liang [e,f,g], Caroline Treins [e,f,g], Mario Pende [e,f,g], Delphine Roussel [a,b,c,d], Michel Le Van Quyen [a,b,c,d], Tomoji Mashimo [h], Takehito Kaneko [i], Takashi Yamamoto [j], Tetsushi Sakuma [j], Séverine Mahon [a,b,c,d], Richard Miles [a,b,c,d], Eric Leguern [a,b,c,d,k], Stéphane Charpier [a,b,c,d], Stéphanie Baulac [a,b,c,d,k,*]

[a] INSERM, U1127, ICM, F-75013 Paris, France
[b] CNRS, UMR 7225, ICM, F-75013 Paris, France
[c] Sorbonne Universités, UPMC Univ Paris 06, UMR S 1127, F-75013 Paris, France
[d] Institut du Cerveau et de la Moelle épinière, ICM, F-75013 Paris, France
[e] Institut Necker-Enfants Malades, CS 61431, Paris, France
[f] INSERM, U1151, F-75014 Paris, France
[g] Université Paris Descartes, Sorbonne Paris Cité, F-75006 Paris, France
[h] Institute of Experimental Animal Sciences, Graduate School of Medicine, Osaka University, Suita 565-0871, Japan
[i] Institute of Laboratory Animals, Graduate School of Medicine, Kyoto University, Kyoto 606-8501, Japan
[j] Department of Mathematical and Life Sciences, Graduate School of Science, Hiroshima University, Hiroshima 739-8526, Japan
[k] Department of Genetics, Pitié-Salpêtrière Hospital, Public Hospital Network of Paris, Paris, France

ARTICLE INFO

Article history:
Received 16 December 2015
Accepted 7 February 2016
Available online 09 February 2016

Keywords:
DEPDC5
Familial focal epilepsy
Focal cortical dysplasia
mTOR
Rapamycin
Knockout

ABSTRACT

DEP-domain containing 5 (*DEPDC5*), encoding a repressor of the mechanistic target of rapamycin complex 1 (mTORC1) signaling pathway, has recently emerged as a major gene mutated in familial focal epilepsies and focal cortical dysplasia. Here we established a global knockout rat using TALEN technology to investigate *in vivo* the impact of *Depdc5*-deficiency. Homozygous *Depdc5*$^{-/-}$ embryos died from embryonic day 14.5 due to a global growth delay. Constitutive mTORC1 hyperactivation was evidenced in the brains and in cultured fibroblasts of *Depdc5*$^{-/-}$ embryos, as reflected by enhanced phosphorylation of its downstream effectors S6K1 and rpS6. Consistently, prenatal treatment with mTORC1 inhibitor rapamycin rescued the phenotype of *Depdc5*$^{-/-}$ embryos. Heterozygous *Depdc5*$^{+/-}$ rats developed normally and exhibited no spontaneous electroclinical seizures, but had altered cortical neuron excitability and firing patterns. *Depdc5*$^{+/-}$ rats displayed cortical cytomegalic dysmorphic neurons and balloon-like cells strongly expressing phosphorylated rpS6, indicative of mTORC1 upregulation, and not observed after prenatal rapamycin treatment. These neuropathological abnormalities are reminiscent of the hallmark brain pathology of human focal cortical dysplasia. Altogether, *Depdc5* knockout rats exhibit multiple features of rodent models of mTORopathies, and thus, stand as a relevant model to study their underlying pathogenic mechanisms.

1. Introduction

DEP-domain containing 5 (*DEPDC5*) is the most common known cause of familial focal epilepsies (nearly 70 unrelated cases described so far). Germline heterozygous inactivating *DEPDC5* mutations are reported in a broad spectrum of focal epileptic syndromes including familial focal epilepsy with variable foci (FFEVF; OMIM 604364), autosomal dominant nocturnal frontal lobe epilepsy (ADNFLE; OMIM 600513), familial temporal lobe epilepsy (FTLE; OMIM 600512) and rare Rolandic epilepsies (OMIM 245570) (Dibbens et al., 2013; Ishida et al., 2013; Lal et al., 2014; Martin et al., 2014; Picard et al., 2014). Patients present focal seizures with variable age at onset, typically during childhood. Brain MRI is usually normal, although within families, some individuals may have a focal cortical dysplasia (FCD; OMIM 607341) (Baulac et al., 2015; Scerri et al., 2015; Scheffer et al., 2014), which is the most common cause of severe, drug-resistant childhood epilepsy. FCD is a malformation of cortical development characterized by cortical dyslamination and the presence of dysmorphic neurons (FCD type IIa) and balloon cells (FCD type IIb) (Blumcke et al., 2011). Recently,

* Corresponding author at: Institut du Cerveau et de la Moelle épinière (ICM), Hôpital de la Pitié-Salpêtrière, 47 bd de l'hôpital, Paris F-75013, France.
E-mail address: stephanie.baulac@upmc.fr (S. Baulac).
[1] Equally contributed.
Available online on ScienceDirect (www.sciencedirect.com).

http://dx.doi.org/10.1016/j.nbd.2016.02.010

germline *DEPDC5* mutations have also been reported in sporadic patients with FCD or hemimegalencephaly (D'Gama et al., 2015).

DEPDC5 does not encode a membrane ion channel, unlike most other epilepsy genes. Instead, DEPDC5 acts *in vitro* as a GTPase-activating protein for RagA/B, and forms part, together with NPRL2 and NPRL3, of the GATOR1 complex to inhibit the mechanistic target of rapamycin complex 1 (mTORC1) pathway (Bar-Peled et al., 2013; Panchaud et al., 2013). Recently, mutations in *NPRL2* and *NPRL3* have also been reported in familial focal epilepsies associated with FCD (Ricos et al., 2016; Sim et al., 2016). The mTORC1 pathway is a major and ubiquitous signaling cascade that regulates multiple cellular processes including cell growth, proliferation and protein synthesis (Laplante and Sabatini, 2012). It is dysregulated in several neurological disorders associated with neurodevelopmental cortical malformations and intractable seizures (Lim and Crino, 2013), including FCD, hemimegalencephaly and tuberous sclerosis complex (TSC; OMIM 191100 and 613254) due to mutations in *TSC1* and *TSC2* genes, encoding inhibitors of the mTORC1 pathway. Numerous rodent models of TSC have been engineered and recapitulate part of the neuropathological features of the disease (Bateup et al., 2013; Meikle et al., 2007). Knockout mice of *Depdc5* partners, *Nprl2* and *Nprl3* have also been recently generated, but have not been explored at the neurological level (Dutchak et al., 2015; Kowalczyk et al., 2012).

To date, the *in vivo* function of Depdc5 in mammals and its role in epilepsy and cortical malformations remain unknown. Here, we generated a global knockout rat of *Depdc5* to model its loss-of-function and investigate the resulting consequences in the brain.

2. Materials and methods

2.1. Animals

Depdc5^{em1kyo} and *Depdc5*^{em2kyo} rats were generated and deposited at the National Bio Resource Project Rat in Japan (www.anim.med.kyoto-u.ac.jp/nbr). Animal care and experimental procedures were approved by the French ministry of research (authorization number 75-1319, project number 03539.02). All efforts were made to minimize the number of animals needed and their suffering.

2.2. TALEN-mediated genome editing in rats

A pair of TALENs targeting exon 2 of rat *Depdc5* (Ensembl: ENSRNOT00000085788) was designed and constructed using a two-step assembly method with a Platinum Gate kit as previously reported (Sakuma et al., 2013). The target sites were located immediately downstream of the ATG start codon. TAL Effector Nucleotide Targeter 2.0 (https://tale-nt.cac.cornell.edu/) did not predict off-target site. We selected the Fisher 344 (F344) rat strain since we previously proved that it is a pertinent model for genetically-determined epilepsies, as exemplified by the *Kcna1* (Ishida et al., 2012), *Scn1a* (Mashimo et al., 2010) or *Lgi1* (Baulac et al., 2012) mutant rats. TALENs were microinjected into fertilized eggs of F344, and then transferred into the oviducts of pseudopregnant Wistar female rats, as previously described (Mashimo et al., 2013). Genomic DNA of founder rats was extracted from tail biopsies. TALEN target site was amplified using the following primers: forward 5′-AGCCTGACATTCTCGCTGTT-3′ and reverse 5′-TCTTGCCCCA CTCATTTACC-3′. Successful germline transmission was confirmed by DNA sequencing of first backcross generation rats. These rats were backcrossed five times with wildtype F344 rats. Genotypes were assessed by the analysis of the PCR products from tail DNA with a high-resolution electrophoresis caliper system. A 267 bp band was detected for wildtype, a 279 bp band for *Depdc5*^{em1kyo} mutant and a 251 bp band for *Depdc5*^{em2kyo} mutant.

2.3. Assessment of embryo vitality

Pregnant rats were injected with lethal dose of pentobarbital sodium (50 mg/kg, i.p.). Embryos were collected by cesarean-section and kept on a warming pad to maintain their body temperature at 37 °C. To assess vitality of embryos aged E12.5 to E16.5, heartbeat was directly observed under a binocular microscope. For E21.5 embryos, cardiac activity was assessed by electromyogram (Neurosoft).

2.4. Rapamycin injection

Rapamycin (LC laboratories) was dissolved at 20 mg/ml in 100% ethanol and stored at −20 °C. Before use, it was diluted to 1 mg/ml in 0.25% Tween 80 and 0.25% polyethylene glycol 300 in PBS. A single dose of 1 mg/kg rapamycin was intraperitoneally injected to pregnant *Depdc5*$^{+/-}$ dams at E13.5 as previously reported (Ma et al., 2014).

2.5. Rat embryonic fibroblast culture

Rat embryonic fibroblasts (REFs) were collected at E13.5 from *Depdc5*$^{+/-}$ interbreeding and cultured in standard medium: Dulbecco's Modified Eagle's Medium (DMEM) (Life Technologies) containing 10% fetal bovine serum and 1% penicillin/streptomycin. Rapamycin (20 nM dissolved in 100% ethanol) was added to Earle's Balanced Salt Solution (EBSS) during the whole starvation period until the harvesting of REFs.

2.6. Cytofluorometric rat embryonic fibroblast size analysis

1×10^6 REFs (passage 6 to 8) were seeded in 100 mm diameter dishes, allowed to proliferate overnight, and then cultured in DMEM without serum for 48 h and starved in EBSS for 3 h. REFs were harvested by gentle trypsinization, washed twice in PBS and fixed in 80% ethanol in PBS. After overnight fixation at −20 °C, fixed cells were washed in PBS, resuspended in DNA staining solution containing 0.20 μg/ml propidium iodide, 100 μg/ml RNaseA and 20 mM EDTA in PBS, and incubated for 30 min at 37 °C. REF soma sizes were analyzed by flow cytometry: the mean cytofluorometric forward scatter (FSC) of minimum 800 stained cells was determined by gating on propidium iodide fluorescence using BD Biosciences FACSCalibur with CellQuest software as previously described (Acosta-Jaquez et al., 2009).

2.7. Western blots

Whole heads of E12.5 embryos were flash-frozen in liquid nitrogen, homogenized with lysing matrix D (MP Biomedicals) in cell lysis buffer (Cell Signaling) containing phosphatase inhibitors and protease inhibitors (Roche). REFs (passage 5) were nutrient-starved with EBSS for 7 h, washed with PBS and then lysed in the same lysis buffer. Similar amount of protein was loaded in each lane in 3–8% Tris–acetate gel for Depdc5 and 10% Bis-Tris–acetate gel (NuPAGE) for phosphorylated S6K1 and rpS6. Western blots were done using the following primary antibodies: anti-DEPDC5 (Cell Signaling, #H6302, 1/100), anti-actin (Sigma Aldrich, #A2066, 1/1000), anti-phosphorylated S6K1 (Thr389) (Cell Signaling, #9205, 1/250) and anti-phosphorylated rpS6 (Ser240/244) (Cell Signaling, #5364, 1/4000). Signal quantification was performed using MultiGauge software (Fuji Film).

2.8. Histology and immunohistochemistry

Whole embryos (E15) were rapidly removed from their chorion and fixed overnight in 4% paraformaldehyde (PFA) in 0.1 M phosphate buffer (PB). Postnatal day (P) P11 and 4 week old rats were injected with a lethal dose of pentobarbital sodium (50 mg/kg, i.p.) and perfused with

4% PFA. Brains were removed, post-fixed in 4% PFA for 24 h, transferred in 30% sucrose in PB 0.1 M, and then stored at −80 °C. Cryostat whole embryo sagittal sections (16 μm thick), P11 brain coronal-cut sections (20 μm thick) and 4 week brain coronal-cut sections (35 μm thick) were collected. To visualize whole embryo gross anatomy and adult brain cortical architecture, sections were stained with Nissl-staining and hematoxylin–eosin using standard techniques. Cell size was determined from Nissl-stained brain sections using NDP.view2 viewer software (Hamamatsu Photonics) to analyze digital slide files. After manual drawing of cell margins, we measured the area from at least 50 large layer IV–V cells. The largest 30 cells per animal were included in the measurements for statistical comparison.

Immunostaining experiments were performed using standard procedure with primary anti-phosphorylated rpS6 Ser240/244 antibody (Cell Signaling, #5364, 1/200) and secondary fluorescent anti-rabbit Alexa 488 antibody (Invitrogen, 1/1000). Nuclei were stained with DAPI. Images were acquired and analyzed through the Nanozoomer software (Hamamatsu photonics). TUNEL assays were performed using In Situ Cell Death Detection Kit (Roche) according to the manufacturer's instructions and images were acquired using a Zeiss apotome.

2.9. In vivo intracellular electrophysiology

Adult rats were anesthetized with 40 mg/kg sodium pentobarbital and 50 mg/kg ketamine (i.p.). Incision and pressure points were repeatedly infiltrated with 2% lidocaine. In line with behavioral EEG experiments (Supplementary data), a small craniotomy was made above the parietal association cortex, allowing combined intracellular and electrocorticographic (ECoG) recordings. The rats were subsequently maintained in a narcotized and sedated state, monitored with the ECoG and heartbeat rate, by injections of fentanyl (3 μg/kg, i.p.) repeated every 20–30 min as previously described (Polack et al., 2009). Rats were paralyzed with gallamine triethiodide (40 mg/2 h, i.m.) and artificially ventilated. Body temperature was maintained at 37 °C with a homeothermic blanket.

ECoG signals were amplified by a differential AC amplifier (Model 1700; A-M Systems), band pass filtered at 1 Hz–1 kHz, and digitized at 3 kHz (Power1401; Cambridge Electronic Design). Intracellular glass micropipettes were filled with 2 M potassium acetate (60–80 MΩ). Current-clamp recordings were amplified using an Axoclamp 900A amplifier (Molecular Devices) in bridge mode, filtered at 6 kHz, and digitized at 20 kHz. Recordings were obtained from pyramidal neurons located at depths ranging from 415 to 1525 μm below the cortical surface (Paxinos, 2005). All data were acquired and analyzed using Spike2 software (Spike2 version 7.16; Cambridge Electronic Design).

Neurons were labeled with neurobiotin (Vector Laboratories) added to the intrapipette solution (1%). At the end of experiments, rats were deeply anesthetized with pentobarbital (200 mg/kg, i.p.) and transcardially perfused with 0.3% glutaraldehyde-4% PFA in PB. The morphology of stained neurons was revealed histochemically as described previously (Polack and Charpier, 2006).

To generate firing frequency versus injected current (F–I) relationships, the firing rate was measured in response to 500 ms depolarizing current pulses of increasing intensity. Each current intensity was applied 3–10 times and the corresponding firing responses were averaged. As previously described (Mahon and Charpier, 2012; Paz et al., 2009), we applied linear regressions to F–I curves and determined the threshold current for action potential (AP) generation, extrapolated as the *x*-intercept of the linear fit, and the neuronal gain, defined as the slope of the F–I curve. The spontaneous firing rate and average membrane potential was calculated from continuous recordings of at least 40 s. Membrane input resistance was calculated as the slope of the linear portion of the voltage–current relationships (500 ms hyperpolarizing pulses of increasing intensity) and the membrane time constant was derived from an exponential decay fit applied to the initial part of the current-induced hyperpolarizations.

Neuronal physiological classes were established as in previous studies (Degenetais et al., 2002; Nunez et al., 1993). Intrinsic bursting cells were characterized either by an initial high-frequency (typically >200 Hz) burst of APs followed by a relatively tonic firing or by consecutive bursts of APs. Regular spiking slow adapting neurons exhibited a sustained discharge of APs with a low frequency adaptation along the current step, while regular spiking fast adapting cells responded to high intensity (typically >0.6 nA) current step by an initial sequence of 3–8 APs restricted to the first 50–100 ms of the response followed by a depolarizing plateau with few or no APs.

2.10. Statistical analysis

Statistical analyses were done with GraphPad and SigmaStat software. The results are presented as mean ± SEM. Normality was assessed by Kolmogorov–Smirnov normality test. Comparisons between two groups were performed by unpaired two-tailed Student's t-test for parametric data and by Mann–Whitney test for non-parametric data. Comparisons between multiple groups were performed by 1-way ANOVA with Tukey's multiple comparison test as post-hoc analysis for parametric data and by a Kruskal–Wallis test for non-parametric data.

3. Results

3.1. Generation of a global Depdc5 knockout rat

DEPDC5-related epilepsies are likely to result from a loss-of-function since the majority of mutations leads to a premature stop codon, targeted by nonsense-mediated mRNA decay (Ishida et al., 2013; Picard et al., 2014). We used transcription activator-like effector nuclease (TALEN)-mediated genome editing to generate a global *Depdc5* knockout rat and to investigate the effects of *Depdc5*-deficiency *in vivo*. TALEN mRNAs targeting exon 2 of rat *Depdc5* were microinjected into fertilized eggs of Fisher 344 (F344) rats, to yield two founder mutant rats named $Depdc5^{em1kyo}$ (c.40_44delins17/p.Gly15*) and $Depdc5^{em2kyo}$ (c.39_55delinsT/p.Lys13fs*8) (Fig. 1A). Successful gene targeting was confirmed by Western blot analysis of whole head lysates from living embryos, with an anti-Depdc5 antibody. Depdc5 protein was absent in homozygous $Depdc5^{em1kyo}$ and $Depdc5^{em2kyo}$ rats, and expression was reduced in heterozygous littermates (Fig. 1B). The homozygous knockout $Depdc5^{em1kyo}$ and $Depdc5^{em2kyo}$ rat strains were therefore indifferently referred to as $Depdc5^{-/-}$, and the heterozygous as $Depdc5^{+/-}$.

3.2. Embryonic lethality and growth delay in $Depdc5^{-/-}$ rats

While $Depdc5^{+/-}$ rats interbred, $Depdc5^{-/-}$ pups were never observed at birth. Deletion of both alleles resulted in *in utero* lethality, as reported in knockout rodents of other genes of the mTORC1 pathway such as *Tsc1* (Kobayashi et al., 2001) and *Tsc2* (Onda et al., 1999; Rennebeck et al., 1998). We assessed the timing of the embryonic lethality by collecting embryos from $Depdc5^{+/-}$ interbred rats at gestation dates between E12.5 and E21.5 (Table 1). All $Depdc5^{-/-}$ embryos were alive until E13.5. However, at E14.5, E15.5 and E16.5, only 50% (7/14), 40% (2/5) and 21% (3/14) of living $Depdc5^{-/-}$ embryos were observed. $Depdc5^{-/-}$ embryos at E13.5-E16.5 were smaller than $Depdc5^{+/+}$ and $Depdc5^{+/-}$ littermates (Fig. 1C). With less developed limbs and optic vesicles, we conclude that global growth delay precedes embryonic lethality observed from E14.5.

Measurements of whole-mount sections from living E14.5 embryos confirmed that $Depdc5^{-/-}$ embryos are smaller ($n = 7$; 6.9 ± 0.2 mm) than $Depdc5^{+/+}$ embryos ($n = 7$; 7.9 ± 0.2 mm) ($P < 0.01$; Mann–Whitney test) (Fig. 1D). TUNEL assays revealed the presence of apoptotic cells in the liver of E14.5 $Depdc5^{-/-}$ embryos (Fig. 1E),

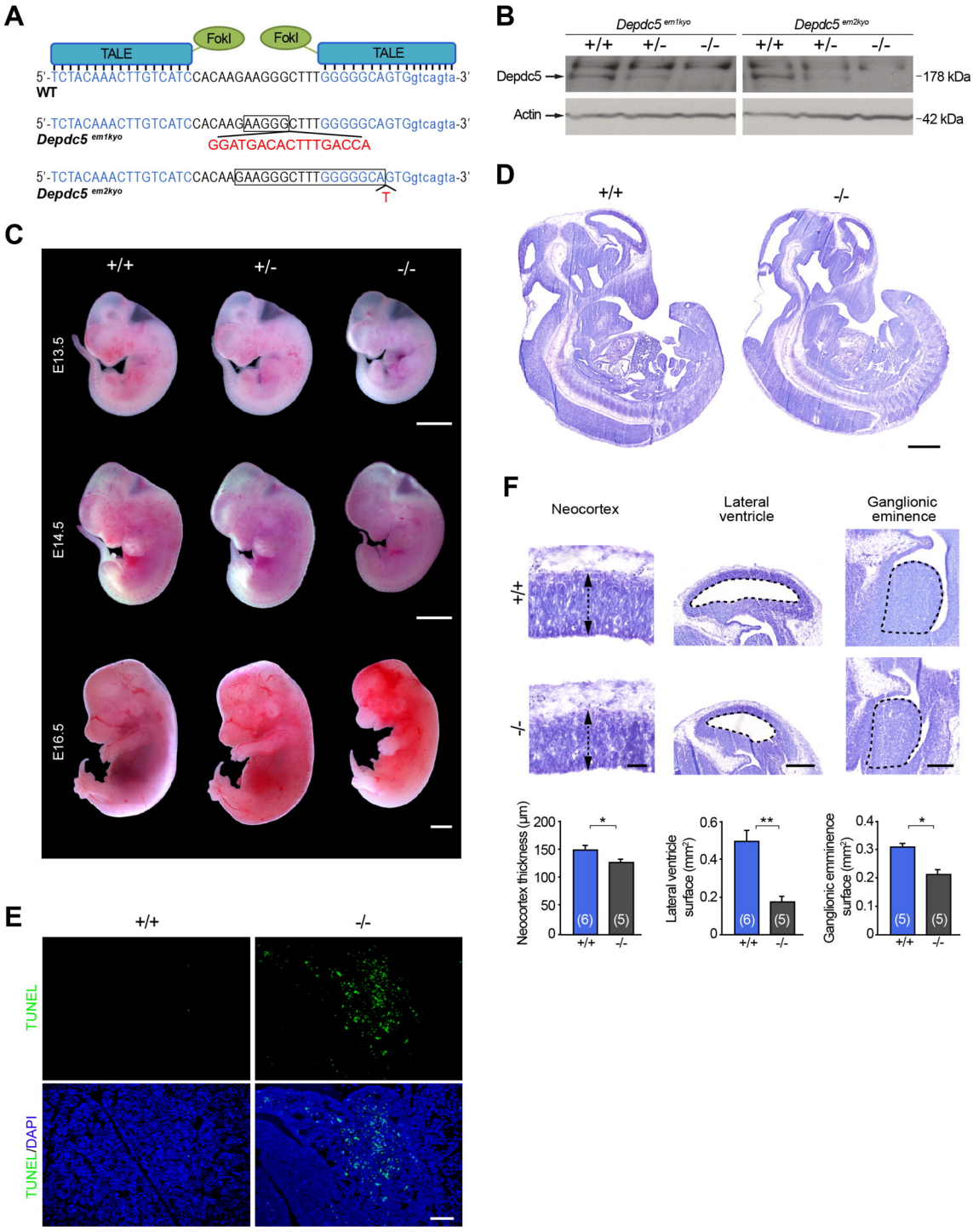

Fig. 1. *Depdc5*$^{-/-}$ rats die embryonically and present growth delay. (A) DNA sequences of wild-type and TALEN-mutated *Depdc5* sequences. TALE: transcription activator-like effector, FokI: restriction endonuclease FokI. TALE binding sequences are shown in blue. Deleted bases are framed, and inserted bases are indicated by the red letters. *Depdc5*^{em1kyo} strain carries a deletion of 5 bp and an insertion of 17 bp, and *Depdc5*^{em2kyo} a deletion of 17 bp and an insertion of 1 bp at the targeted site. (B) Western blots of head lysates (60 µg of protein each) from living embryonic day 12.5 (E12.5) embryos derived from *Depdc5*^{em1kyo} and *Depdc5*^{em2kyo} strains with *Depdc5* and actin antibodies. The *Depdc5* specific band is indicated by an arrow, the upper band is nonspecific. (C) Representative picture of embryos from three litters at E13.5, E14.5 and E16.5. Picture of E16.5 embryo is composed of two images. Scale bar: 2 mm. (D) Representative Nissl-stained whole body sagittal sections of living E14.5 (*Depdc5*$^{+/+}$, n = 7; *Depdc5*$^{-/-}$, n = 7) embryos. Scale bar: 1 mm. (E) Representative images of TUNEL staining on fetal liver from living E14.5 (*Depdc5*$^{+/+}$, n = 3; *Depdc5*$^{-/-}$, n = 3) embryos. Scale bar: 100 µm. (F) Higher magnification view of brain regions on Nissl-stained sections. From left to right panel: neocortex, lateral ventricle and ganglionic eminence. Histogram indicates quantification of neocortical thickness (indicated by black arrows), lateral ventricular and ganglionic eminence surfaces (dashed-lines). Scale bar: 50 µm, 500 µm and 250 µm respectively. Number of embryos is indicated in brackets. Error bars represent mean ± SEM. n.s., not significant; *$P < 0.05$; **$P < 0.01$ (Mann–Whitney test).

suggesting important impairment of this organ, which may be the cause of premature death. This result reveals that Depdc5 plays an important role in liver development, and recalls the liver defects observed in knockout mice of *Depdc5* partners, *Nprl2* and *Nprl3* (Dutchak et al., 2015; Kowalczyk et al., 2012) acting in the GATOR1 complex. The cerebral neocortical structures of embryonic *Depdc5*$^{-/-}$ rats were also

Table 1
Viability of *Depdc5*$^{-/-}$ embryos according to age.

Age	Number of embryos			
	Total	+/+	+/−	−/−
E12.5	28	7	15	6 (100%)
E13.5	44	15	21	8 (100%)
E14.5	75	24	37	14 (50%)
E15.5	51	17	29	5 (40%)
E16.5	95	16	65	14 (21%)
E21.5	31	4	25	2 (0%)
P5	96	35	61	0 (0%)

E, embryonic day; P, postnatal day; numbers in parentheses refer to percentage of living *Depdc5*$^{-/-}$ embryos with heartbeat detected.

affected, in line with the role of *DEPDC5* in malformations of the cortical development in humans. Analysis of Nissl-stained whole-embryo sections revealed the neocortex was thinner and the surfaces of both lateral ventricles and ganglionic eminences were smaller in *Depdc5*$^{-/-}$ embryos than in their *Depdc5*$^{+/+}$ littermates (Fig. 1F).

3.3. Prenatal rapamycin rescues growth delay and embryonic lethality in *Depdc5*$^{-/-}$ rats

Previous *in vitro* studies have reported that Depdc5 acts as a repressor of the mTORC1 signaling pathway (Fig. 2A) (Bar-Peled et al., 2013; Panchaud et al., 2013). If mTORC1 pathway were involved in the embryonic lethality of *Depdc5*$^{-/-}$ rats, prenatal administration of the mTORC1 inhibitor rapamycin might rescue their phenotype. We injected a single

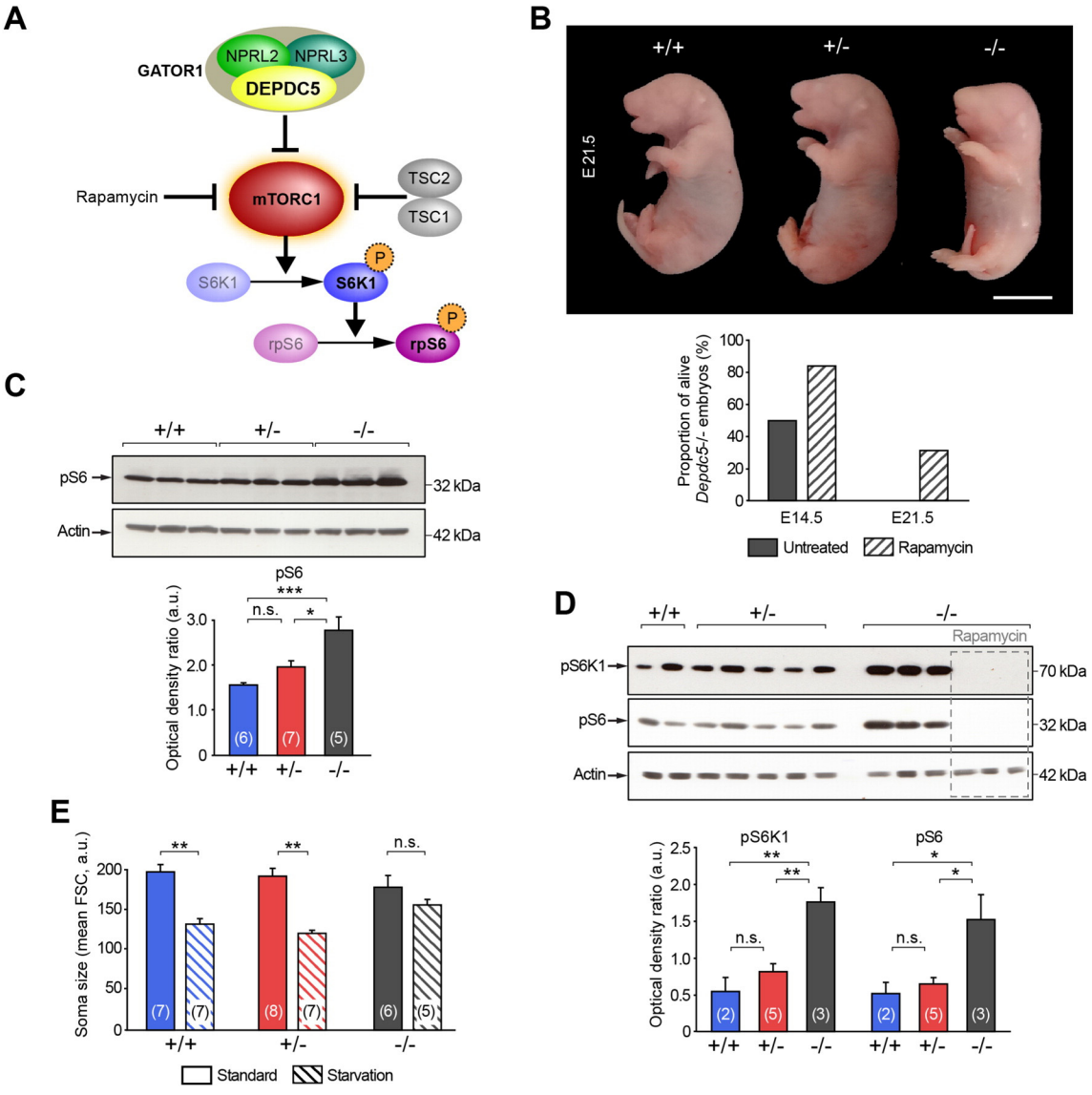

Fig. 2. mTORC1 pathway is upregulated in *Depdc5*$^{-/-}$ embryos. (A) Schema of the *Depdc5*-mTORC1 signaling pathway. (B) Top panel: Representative picture of living E21.5 embryos treated with rapamycin (*Depdc5*$^{+/+}$, n = 14; *Depdc5*$^{+/-}$, n = 23; *Depdc5*$^{-/-}$, n = 4). Scale bar: 1 cm. Bottom panel: Histogram showing the percentage of living *Depdc5*$^{-/-}$ embryos treated or not with prenatal rapamycin. (C) Top panel: Western blot of brain lysates (30 μg of protein) of E12.5 littermate embryos with phosphorylated rpS6 on Ser240/244 (pS6) and actin antibodies. Bottom panel: Histogram of densitometry analysis of pS6 normalized with actin from two independent Western blots. (D) Top panel: Western blot of REF lysates (15 μg of protein) derived from littermate embryos with phosphorylated S6K1 on Thr389 (pS6K1), phosphorylated rpS6 on Ser240/244 (pS6) and actin antibodies after amino acid starvation, with or without rapamycin. Bottom panel: histogram of densitometry analysis of pS6K1 and pS6 normalized with actin from above Western blot. (E) REF soma sizes, expressed as mean cytofluorometric forward scatter (FSC), in standard or amino acid starvation conditions from two independent cytofluorometric REF sizes analysis. Number of embryos is indicated in brackets. Error bars represent mean ± SEM. a.u., arbitrary units; n.s., not significant; $^{*}P < 0.05$; $^{**}P < 0.01$; $^{***}P < 0.001$ (1-way ANOVA and Tukey's multiple comparison post-hoc tests).

dose of rapamycin (1 mg/kg) to pregnant *Depdc5*$^{+/-}$ dams at E13.5, as previously reported in a *Tsc1* knockout mouse model (Ma et al., 2014). The proportion of living *Depdc5*$^{-/-}$ embryos increased from 50% to 83% at E14.5 with this treatment. At the projected birth date E21.5, 31% (4/13) of living *Depdc5*$^{-/-}$ rats were obtained after prenatal rapamycin treatment (Fig. 2B, bottom). The body length of E21.5 rescued *Depdc5*$^{-/-}$ embryos ($n = 4$; 3.8 ± 0.2 cm) was similar to that of *Depdc5*$^{+/+}$ ($n = 10$; 3.7 ± 0.3 cm) and *Depdc5*$^{+/-}$ ($n = 11$; 3.9 ± 0.3 cm) littermate embryos ($P > 0.5$; Kruskal–Wallis test), indicating that rapamycin also reversed growth delay. While rapamycin enhanced embryonic survival of *Depdc5*$^{-/-}$ rats, they showed global edema, and died shortly after birth from impaired maternal–pup interaction. Rapamycin treatment earlier or later than E13.5 did not improve *Depdc5*$^{-/-}$ embryo survival (data not shown). The appearance and body length of treated *Depdc5*$^{+/+}$ and *Depdc5*$^{+/-}$ rats were similar to those of untreated littermates, indicating that rapamycin had no major adverse effects on control rats (Fig. 2B, top). This results provided evidence that mTORC1 pathway is involved in growth delay and embryonic lethality in *Depdc5*$^{-/-}$ embryos.

To further validate an mTORC1 activity-dependent mechanism, we assessed at the molecular level whether mTORC1 is upregulated in the brains of *Depdc5*$^{-/-}$ embryos. Thus we monitored by Western blot mTORC1 activation through the phosphorylation state of one of its downstream effector, the ribosomal protein S6 (rpS6, on Ser240/244). rpS6 phosphorylation level was significantly enhanced in brain lysates of E12.5 *Depdc5*$^{-/-}$ embryos compared to *Depdc5*$^{+/+}$ and *Depdc5*$^{+/-}$ littermates, and tended to be higher in *Depdc5*$^{+/-}$ than in *Depdc5*$^{+/+}$ embryos (Fig. 2C). This indicates constitutive activation of mTORC1 in the brains of *Depdc5*-deficient embryos with a gene dosage effect such that levels of phosphorylated rpS6 are higher when both copies of *Depdc5* are deleted.

3.4. Upregulation of mTORC1 in *Depdc5*$^{-/-}$ cultured fibroblasts after amino acid starvation

mTORC1 pathway is sensitive to amino acid starvation. Since *in vitro* data from mammalian cell lines suggests this sensitivity is abolished by *Depdc5* knockdown (Bar-Peled et al., 2013), we examined the effect of *Depdc5*-deficiency on primary rat embryonic fibroblasts (REFs). REFs derived from *Depdc5*$^{+/-}$ interbreeding let us compare mTORC1 activity in standard or amino acid-deprived culture media. mTORC1 activity was monitored by the phosphorylation of two downstream effectors: p70S6 kinase 1 (S6K1, on Thr389) and the S6K1 substrate rpS6 (on Ser240/Ser244) as previously reported (Dutchak et al., 2015; Efeyan et al., 2014; Liang et al., 2014). In standard medium, Western blots of REF lysates indicated that phosphorylation levels of S6K1 and rpS6 were similar across genotypes (data not shown). However, after amino acid starvation, phosphorylation states of both S6K1 and rpS6 were consistently increased in REF lysates derived from *Depdc5*$^{-/-}$ embryos compared to those from *Depdc5*$^{+/+}$ and *Depdc5*$^{+/-}$ embryos (Fig. 2D). Rapamycin treatment of REFs derived from *Depdc5*$^{-/-}$ embryos abolished S6K1 and rpS6 phosphorylation, confirming that Depdc5 negatively regulates mTORC1 activity. We also compared mTORC1 activity in REFs derived from *Depdc5*$^{+/-}$ embryos to REFs derived from *Depdc5*$^{+/+}$ embryos to assess the effect of the lack of one copy of *Depdc5* on the pathway activity. Semi-quantification of Western blot suggested a tendency to increased phosphorylation states of S6K1 and rpS6 in REFs derived from *Depdc5*$^{+/-}$ compared to *Depdc5*$^{+/+}$, but did not reach significant levels (Fig. 2D). This result is in line with the data obtained above in brain lysates (Fig. 2C), showing robust mTORC1 upregulation in *Depdc5*$^{-/-}$ embryos, and more subtle effects in *Depdc5*$^{+/-}$ embryos. A similar upregulation was obtained in REFs derived from a knockout mouse for *Nprl2* (Dutchak et al., 2015), one of the two Depdc5 partners in the GATOR1 complex.

Acting via S6K1 and rpS6, mTORC1 is a pivotal regulator of cell size. We therefore assessed the impact of an mTORC1 upregulation on the soma size of REFs derived from *Depdc5*$^{+/+}$, *Depdc5*$^{+/-}$ and *Depdc5*$^{-/-}$ embryos, in standard or amino acid starvation condition using flow cytometry analysis. In standard medium, REF soma sizes did not differ significantly between genotypes. After amino acid starvation, both *Depdc5*$^{+/+}$ and *Depdc5*$^{+/-}$ derived REFs were reduced in size while *Depdc5*$^{-/-}$ derived REFs remained unchanged (Fig. 2E). These data indicate that Depdc5 is necessary to control the cell growth by repressing mTORC1 pathway during amino acid starvation.

3.5. Brain cortical structural abnormalities in *Depdc5*$^{+/-}$ rats

Heterozygous *Depdc5*$^{+/-}$ rats displayed no differences in gross anatomy, fertility and rates of weight gain compared to control littermates (Supplementary data, Fig. 1A). Some inactivating deletions in *DEPDC5* may be associated with ovarian cancers and glioblastomas (Cancer Genome Atlas: http://cancergenome.nih.gov/). Besides, TSC patients develop tumors associated with an increased mTORC1 activity (Onda et al., 1999). We therefore asked whether *Depdc5*-deficiency promotes tumor development. No evidence for tumors was apparent in *Depdc5*$^{+/-}$ rats whole body at ages greater than 12 months ($n = 8$). Furthermore, we detected no differences between *Depdc5*$^{+/+}$ and *Depdc5*$^{+/-}$ littermate rats survival (up to 18 months).

We next assessed possible defects in brain cortical architecture of *Depdc5*$^{+/-}$ rats, since heterozygous *DEPDC5* mutations may cause cortical malformation such as FCD type II in humans (Baulac et al., 2015; D'Gama et al., 2015; Scerri et al., 2015) with an increased cortical thickness, blurred gray/white matter demarcation and cortical dyslamination as well as dysmorphic neurons in FCD type IIa, and balloon cells in FCD type IIb (Blumcke et al., 2011). We found that the brain-to-body weight ratios of *Depdc5*$^{+/+}$ and *Depdc5*$^{+/-}$ rats were similar (Supplementary data, Fig. 1B). Nissl-staining of coronal brain sections of *Depdc5*$^{+/-}$ rats revealed no major defects in the structural brain organization at 4 weeks (Fig. 3A) and 23 weeks (data not shown). Cerebral cortical thickness did not differ between *Depdc5*$^{+/+}$ ($n = 6$, 1.22 ± 0.01 mm) and *Depdc5*$^{+/-}$ ($n = 6$, 1.21 ± 0.01 mm) rats ($P > 0.05$; Mann–Whitney test), neither in gray/white matter boundaries (Fig. 3A). In contrast, the delimitations between the six cortical layers were less distinct in *Depdc5*$^{+/-}$ rats, particularly between layers I–II (ectopic neurons were observed in layer I) and V–VI (Fig. 3B). These aberrantly positioned cells suggest that neuronal migration was perturbed because of *Depdc5* haploinsufficiency. Furthermore, Nissl and hematoxylin & eosin staining revealed the presence of enlarged cells throughout the cortex of *Depdc5*$^{+/-}$ rats, especially in layers IV–V (approximately 15 cells/mm^2). These cells consisted of both balloon-like cells resembling those seen in FCD type IIb, with no Nissl substance and an eosinophilic cytoplasm (Fig. 3C, top), and of cytomegalic dysmorphic neurons, with an aggregated Nissl substance displaced towards the cell membrane, as seen in FCD type IIa and IIb (Fig. 3C, middle). Balloon-like cells and cytomegalic dysmorphic neurons were never observed in *Depdc5*$^{+/+}$ littermates. To confirm a difference in neuronal cell size, we measured the soma size of pyramidal neurons in cortical layers IV–V from Nissl-stained sections. The soma size of the cytomegalic dysmorphic neurons present in cortical layers IV-V of *Depdc5*$^{+/-}$ rats were significantly greater than the largest pyramidal cell in *Depdc5*$^{+/+}$ rats from same layers, with an average area size increase of ~30% (Fig. 3C, bottom).

3.6. Effects of rapamycin treatment on cytomegalic dysmorphic neurons

Are these cytomegalic dysmorphic neurons linked to mTORC1 upregulation? We pursued this question by immunostaining for phosphorylated rpS6 (on Ser240/244) in brain sections from 4 week-old *Depdc5*$^{+/+}$ and *Depdc5*$^{+/-}$ rats. A basal level of rpS6 phosphorylation was detected in normal-appearing (non-cytomegalic) pyramidal neurons from *Depdc5*$^{+/+}$ and *Depdc5*$^{+/-}$ rats (Fig. 3D, left). In contrast, phosphorylated rpS6 staining of the majority of cytomegalic

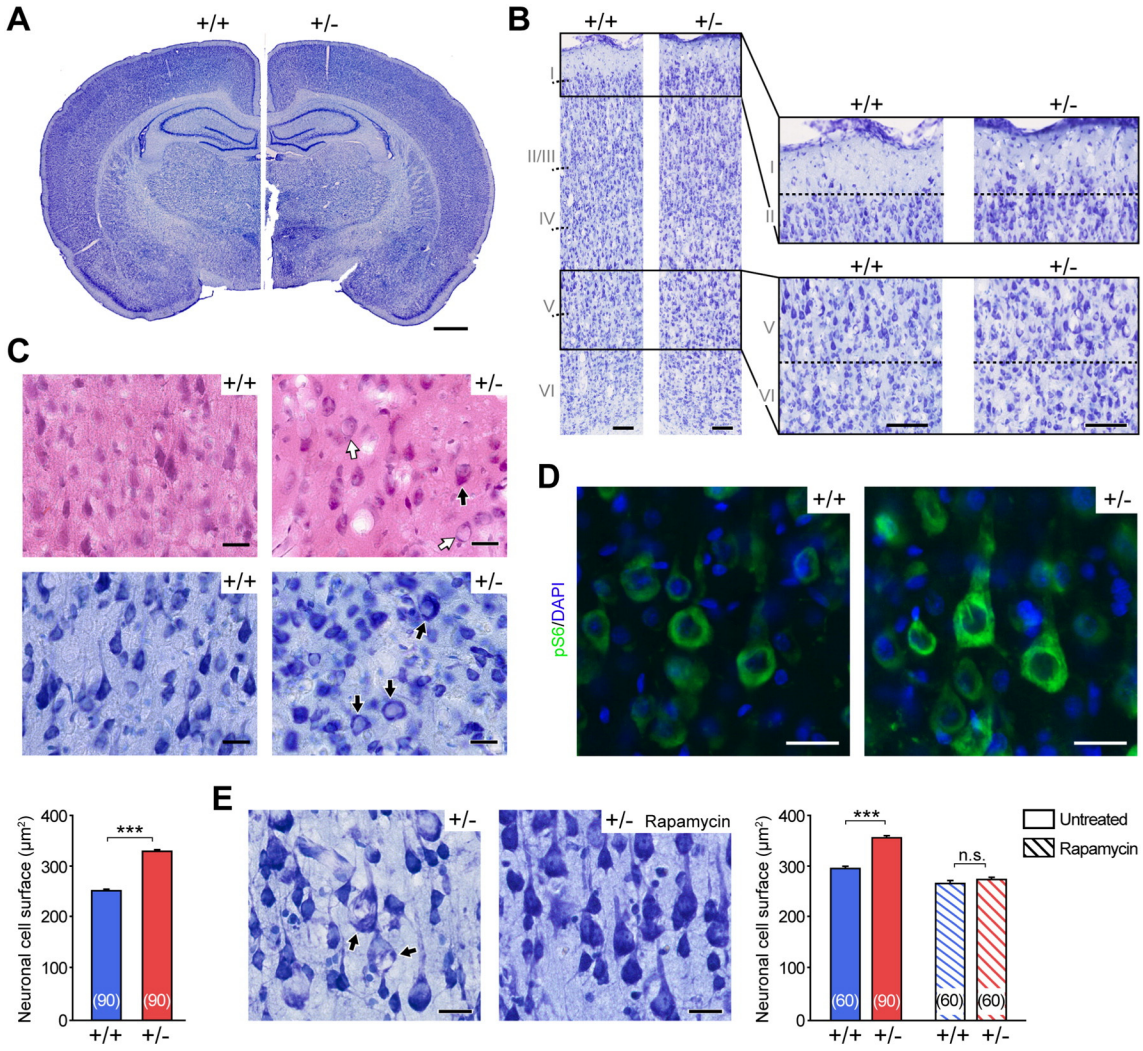

Fig. 3. *Depdc5*$^{+/-}$ rats develop brain cortical abnormalities. (A to D) Representative brain anatomy of 4-week old littermate rats (*Depdc5*$^{+/+}$, n = 3; *Depdc5*$^{+/-}$, n = 3). (A) Nissl-stained whole-brain coronal sections showing the organization of cortical layers. Scale bar: 1 mm. (B) Higher magnification of panel A showing the organization of cortical layers, with enlargement of boundaries between layers I–II and V–VI. scale bar: 100 µm. (C) Top panel; Hematoxylin–eosin staining showing dysmorphic neurons (black arrows) and balloon-like cells (white arrows) in cortical layer V. Middle panel; Nissl staining showing dysmorphic neurons (black arrows) in cortical layer V. Scale bar: 25 µm. Bottom panel; quantitative neuronal size analysis from cortical layers IV–V of 4-week old littermate rats (n = 30 cells per animal). Student's t-test was used. (D) Immunohistochemistry of enlarged cells with intense phosphorylated rpS6 on Ser240/244 (pS6) signals in *Depdc5*$^{+/-}$ rats. Scale bar: 25 µm. (E) Representative brain anatomy of P11 old (*Depdc5*$^{+/-}$, n = 3; *Depdc5*$^{+/-}$ treated with rapamycin, n = 2) rats. Left and middle panel; Nissl staining showing dysmorphic neurons (black arrows) in *Depdc5*$^{+/-}$ and normal appearing neurons in *Depdc5*$^{+/-}$ treated with rapamycin in cortical layer V. Scale bar: 20 µm. Right panel; quantitative neuronal size analysis from cortical layers IV–V of P11 rapamycin untreated and treated rats (n = 30 cells per animal). Kruskall–Wallis test was used. Number of cells is indicated in brackets. Error bars indicate ± SEM. n.s., not significant; ***$P < 0.001$.

dysmorphic neurons in layers IV–V was more intense than nearby normal-appearing cells (Fig. 3D, right). Altogether these results suggest that increased cell size is caused by hyperactivation of the mTORC1 pathway.

To evaluate if rapamycin could prevent the emergence of cytomegalic and dysmorphic neurons, pregnant *Depdc5*$^{+/-}$ dams were treated with rapamycin as described above. We focused the analysis on littermate rats aged P11. At P11, cytomegalic dysmorphic neurons were present in *Depdc5*$^{+/-}$ (Fig. 3E, left), but not in *Depdc5*$^{+/+}$ littermates. Standard histological analysis of cortical sections from the rapamycin-treated *Depdc5*$^{+/-}$ rats showed rapamycin rescued cortical abnormalities (Fig. 3E, middle). Quantitative measurements revealed a significant reduction in cell size and Nissl aggregates after rapamycin treatment in *Depdc5*$^{+/-}$ neurons (reduced from ~30% when compared with untreated *Depdc5*$^{+/-}$ neurons) (Fig. 3E, right). Thus, *Depdc5* haploinsufficiency results in enhanced cell size and dysmorphy of neurons that are preventable by rapamycin treatment, demonstrating an mTORC1-dependent mechanism.

3.7. Changes in pyramidal cell electrophysiology in *Depdc5*$^{+/-}$ rats

We searched for possible spontaneous epileptic behavior in *Depdc5*$^{+/-}$ rats, since heterozygous *DEPDC5* mutations cause seizures in Human. A video-based approach revealed no clonic or convulsive seizure-like behavior in young (P10 to P28), juvenile (5 to 11 week-old) or adult (12 to 20 week-old) rats (*Depdc5*$^{+/-}$, $n = 18$; *Depdc5*$^{+/+}$, $n = 10$). We did not detect neither seizure-like events nor interictal activity by electroencephalogram in young, juvenile and adult rats (*Depdc5*$^{+/-}$, $n = 12$; *Depdc5*$^{+/+}$, $n = 9$) (Supplementary data, Fig. 2). In line with this result, we note that all studies on heterozygous global knockout rodents of *Tsc1* and *Tsc2* also reported the absence of spontaneous seizures (Lasarge and Danzer, 2014), to the exception of one global *Tsc1*$^{+/-}$ mouse model that displays ictal events during a short postnatal window (<P19) (Lozovaya et al., 2014).

We asked whether *Depdc5*-deficiency could alter the intrinsic properties and excitability of single neurons using *in vivo* simultaneous electrocorticographic (ECoG) and intracellular recordings of cortical

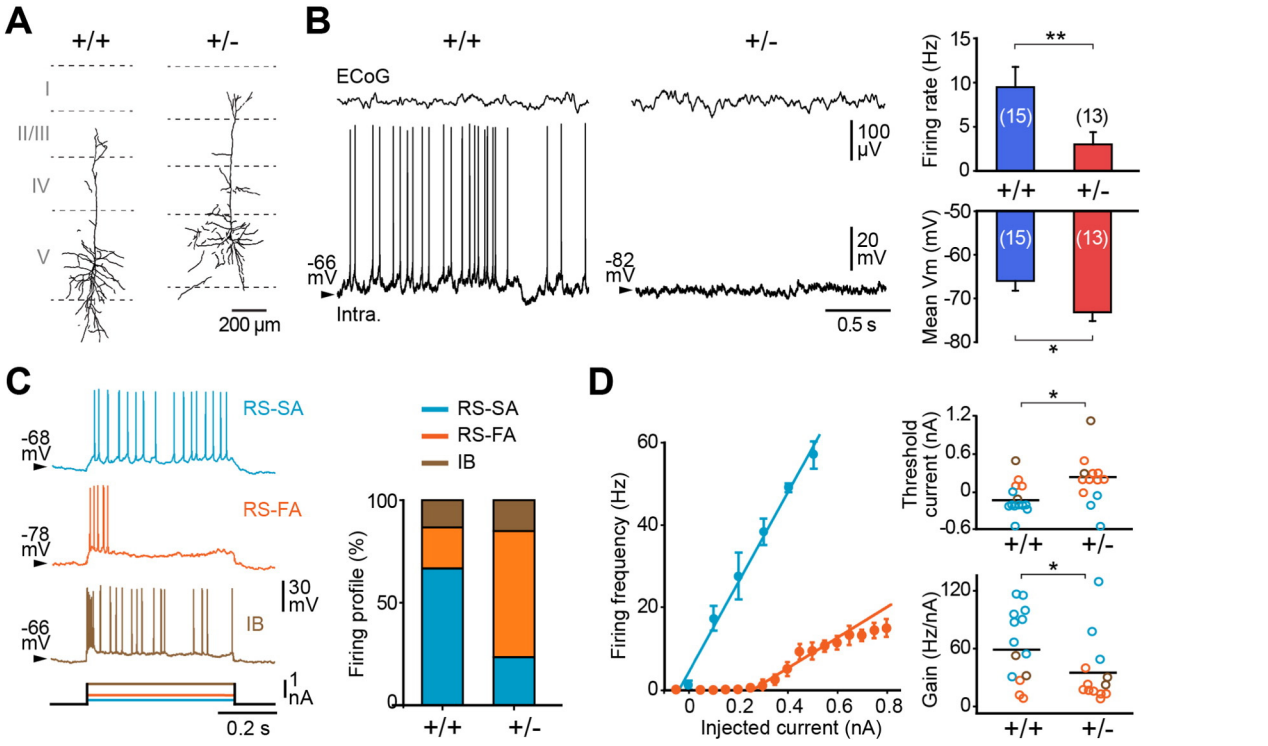

Fig. 4. *Depdc5*$^{+/-}$ neurons exhibit altered neuronal electrophysiological properties. (A) Anatomical reconstruction of neurobiotin-injected layer V pyramidal neurons (*Depdc5*$^{+/+}$, n = 6; *Depdc5*$^{+/-}$, n = 10). (B) Left panel: Spontaneous intracellular activity of a layer V cortical neuron and ECoG signals from *Depdc5*$^{+/+}$ and *Depdc5*$^{+/-}$ rats. Right panel: summary data of spontaneous firing rate and average membrane potential (Vm). (C) Left panel: Intracellular responses to 500 ms suprathreshold current pulses from a regular spiking slow-adapting (RS-SA), a regular spiking fast-adapting (RS-FA) and an intrinsic bursting (IB) neuron. Right panel: relative proportion of neurons displaying RS-SA, RS-FA or IB intrinsic firing profiles. (D) Relationship between the intrinsic firing profile and the transfer function of cortical pyramidal neurons. Left panel: representative F–I relationships for two neurons (RS-SA and RS-FA from *Depdc5*$^{+/+}$ and *Depdc5*$^{+/-}$ rats, respectively). Right panel: summary data of current threshold and neuronal gain values highlighting the differences between the two genotypes. Color-coding is as in panel C. Number of neurons is indicated in brackets. n.s., not significant; $^{*}P < 0.05$; $^{**}P < 0.01$ (Student's t-test or Mann–Whitney test). Blue and red is indicated for +/+ and +/- respectively (shown in panel B). Light blue, orange and brown is indicated in panel C.

neurons (n = 15 cells from 9 *Depdc5*$^{+/+}$ rats, and 13 cells from 8 *Depdc5*$^{+/-}$ rats, with typical pyramidal morphology). Spontaneously, neurons from *Depdc5*$^{+/-}$ rats were significantly more hyperpolarized and had a lower firing rate (9 out of 13 neurons were silent) than *Depdc5*$^{+/+}$ rat's neurons (Fig. 4A and B). This discrepancy was not associated with changes in passive properties since the membrane input resistance and time constant were similar between *Depdc5*$^{+/-}$ and *Depdc5*$^{+/+}$ neurons (Supplementary data, Fig. 3). Furthermore, action potential parameters, including voltage threshold, amplitude, maximum rate-of-rise and total width, were not significantly different ($P > 0.05$ for each parameter, Student's t test and Mann–Whitney tests) between genotypes.

We next investigated the firing patterns of *Depdc5*$^{+/-}$ neurons in response to current pulse injections. We recorded three classes of pyramidal neurons with distinct firing patterns: intrinsic bursting (IB), regular spiking slow adapting (RS-SA) and regular spiking fast adapting (RS-FA) (Fig. 4C, left). Pyramidal cells of *Depdc5*$^{+/+}$ rats displayed a typical ratio for these different firing profiles: IB 13%, RS-SA 66% and RS-FA 20% (Degenetais et al., 2002; Nunez et al., 1993). In contrast, the relative proportion of RS-FA neurons was considerably higher in *Depdc5*$^{+/-}$ rats: IB 15%, RS-SA 23% and RS-FA 61% (Fig. 4C, right). These divergences were in line with differences in transfer functions, measured as the mean firing frequency induced by depolarizing current pulses of increasing intensity. The minimal current to induce firing in RS-FA neuron was much higher and the slope of the transfer function was lower than that for RS-SA neurons (Fig. 4D, left). With increased numbers of RS-FA neurons, *Depdc5*$^{+/-}$ neurons were on average significantly less responsive to excitatory inputs (Fig. 4D, right). We note however that cytomegalic neurons observed in *Depdc5*$^{+/-}$ rat brains, which were not recorded here, may have pro-epileptic properties, as suggested in humans (Abdijadid et al., 2015). Thus, *Depdc5*-deficiency impacts both the overall intrinsic properties and excitability of cortical pyramidal neurons.

4. Discussion

Humans that carry heterozygous loss-of-function mutations of *DEPDC5* exhibit focal epileptic syndromes with or without developmental brain cortical malformations. We introduced loss-of-function *Depdc5* mutations in F344 rats to mimic human haploinsufficiency. This novel knockout animal model shows Depdc5 is required for global growth and embryonic viability. Heterozygous deletion of *Depdc5* in rat leads to brain cortical abnormalities with cytomegalic and dysmorphic phosphorylated rpS6-positive neurons due to upregulation of the mTORC1 pathway.

In vitro, Depdc5 represses the activity of the amino-acid sensing branch of the mTORC1 pathway (Bar-Peled et al., 2013; Panchaud et al., 2013). Thus, we assessed *in vivo* how mTORC1 signaling is affected by *Depdc5*-deficiency. Deletion of both *Depdc5* alleles induced an embryonic lethality, observed from E14.5, preceded by global growth delay, consistent with the ubiquitous expression of Depdc5 in whole body. Rapamycin, a specific mTORC1 inhibitor, when administered prenatally, rescued the growth defect and improved the survival of *Depdc5*$^{-/-}$ embryos, providing evidence of a direct link between Depdc5 and mTORC1 signaling cascade. We further demonstrated that deletion of both alleles of *Depdc5* produces increased phosphorylation of mTORC1 downstream effectors associated with enlargement of soma size of cultured rat embryonic fibroblasts (REFs). Our data also show that REFs derived from *Depdc5*$^{-/-}$ embryos did not repress mTORC1 activity during amino acid starvation, confirming mTORC1 senses amino acid levels via Depdc5. Altogether, both the rapamycin

rescue and the upregulation of the mTORC1 pathway, demonstrates that *Depdc5*-deficiency leads to early developmental mTORC1-dependant defects. Similar effects are described in global and conditional knockout mouse models of mTORopathies including *Tsc1* (Anderl et al., 2011; Ma et al., 2014) and *Tsc2* (Way et al., 2012). We note, however that the phenotype of *Depdc5*-deficient rats is less severe since *Tsc1* and *Tsc2* rodent models succumb earlier, during mid-gestation (from E9.5).

Lack of a single *Depdc5* copy reflects the genotype of patients who are heterozygous for *DEPDC5* mutations. In rats, such a loss induced alterations in the neuronal development including aberrant cortical lamination, indicative of neuronal migration defects. Furthermore *Depdc5* haploinsuffiency also conduced to the presence, throughout the cortex of *Depdc5*$^{+/-}$ rats (from age P11) of cells, resembling cytomegalic dysmorphic neurons and balloon cells in FCD type II patients, which typically exhibit an increased cell soma size of 50–100% (Lim and Crino, 2013). We furthermore demonstrated that these morphological changes were due to mTORC1 pathway hyperactivity, and that prenatal administration of rapamycin was effective in preventing their apparition. Thus this model shares neuropathological hallmarks with sporadic FCD type II patients presenting dysmorphic cortical neurons (Baybis et al., 2004; Miyata et al., 2004). Accordingly, phosphorylated rpS6-positive dysmorphic neurons were also seen in postoperative brain tissue from a FCD type II patient with a *DEPDC5* mutation (Scerri et al., 2015). These brain pathological findings also parallel the phenotype in *Tsc1* conditional knockout mouse with enlarged dysmorphic neurons associated with increased mTORC1 activity (Meikle et al., 2007). Similar to the other *Tsc1* and *Tsc2* brain-specific knockout rodent models (Goto et al., 2011; Meikle et al., 2008; Tsai et al., 2013), rapamycin treatment was effective in this model and improved the cortical abnormalities. This result confirms an mTORC1-dependent mechanism leading to the features reminiscent of FCD in heterozygous *Depdc5*$^{+/-}$ rats.

However, despite these developmental cortical abnormalities, we did not detect spontaneous seizures in *Depdc5*$^{+/-}$ rats. In *Depdc5*$^{+/-}$ F344 rats, as in most other *Tsc1*$^{+/-}$ and *Tsc2*$^{+/-}$ global knockout rodent models, gene dosage effects may ensure that deletion of a single copy is not sufficient to trigger seizures. Therefore, we speculate that investigation of epileptic activity will necessitate viable homozygous animals using conditional brain-specific knockout approaches, as done in other studies with *Tsc1* and *Tsc2* rodent models (Bateup et al., 2013; Meikle et al., 2007). Indeed, brain-specific conditional *Tsc1*$^{-/-}$ and *Tsc2*$^{-/-}$ knockout mouse consistently exhibit spontaneous epileptic seizures.

We then asked if and how the deletion of *Depdc5* could alter the electrophysiological properties of cortical neurons. Intracellular recordings in *Depdc5*$^{+/-}$ rats revealed increased proportion of pyramidal neurons with a peculiar firing pattern (RS-FA type) consisting of hyperpolarized membrane potentials and a response restricted to the initial part of depolarizing current steps. The molecular cascade that links Depdc5 to the regulation of the physiological neuronal types remains to be addressed. Yet, we hypothesize that the increased proportion of RS-FA type cells is plausibly caused by potentiation of potassium (K^+) channels activity through mTORC1 pathway activity. Accordingly, it has been shown that elevated levels of mTOR increase K^+ currents, leading to neuronal electrical properties reminiscent of those measured in RS-FA neurons (Yang et al., 2012). Enhanced mTORC1 activity has been shown to regulate neuronal excitability notably by direct actions on ion channel expression (Lasarge and Danzer, 2014). Other genes associated with inherited focal epilepsies include a neuronal (Slack) sodium-activated potassium channel subunit (*KCNT1*) as well as three neuronal nicotinic acetylcholine receptor subunit genes (*CHRNA4*, *CHRNA2*, *CHRNB2*). Therefore, it will be relevant to address whether downstream effects of *Depdc5*-deficiency include direct or indirect actions on Slack potassium channels or the nicotinic receptors, underlying a common pathway for familial focal epilepsies. Alternatively, Depdc5 may have a role in the physiological late differentiation of the various subtypes of pyramidal neurons.

5. Conclusions

This study highlights the critical role of Depdc5 in development, and provides proof that Depdc5 inhibits mTORC1 signaling *in vivo*. *Depdc5*$^{-/-}$ knockout rats exhibit several features common to other mTORopathy rodent models, such as global growth delay, embryonic lethality, mTORC1 upregulation and benefit of rapamycin rescue. *Depdc5*$^{+/-}$ rats display developmental neuropathological abnormalities such as cytomegalic dysmorphic phosphorylated rpS6-positive neurons and brain cortical dyslamination, reminiscent of those induced by *DEPDC5* mutations in humans with FCD type II. These neuropathological abnormalities appeared during the development and were rescued by prenatal rapamycin treatment. Thus, this study provides evidence that rapamycin can induce significant physiologic improvement *in vivo* in a model of *Depdc5*-deficiency. The poor efficacy of conventional antiepileptic drugs (Baulac et al., 2015; Picard et al., 2014) imposes a switch to more effective drugs with targets based on a better understanding of the physiopathological mechanisms involved. The mTORC1 inhibitor rapamycin, which reduces seizures in TSC patients with intractable epilepsy (Wiegand et al., 2013), may serve as a starting point to develop novel molecules to treat patients with diverse mTORopathies.

Conflicts of interest

The authors have no conflicts of interest to declare.

Funding

This work was supported by the program “Investissements d'avenir” ANR-10-IAIHU-06, Fondation pour la Recherche sur le Cerveauand Fondation pour la Recherche Médicale (équipe FRM DEQ2015033).

Acknowledgments

The authors thank Jerome Garrigue for genotyping, Morgane Boillot for helping with EEG and SeizureScan recordings, Eric Noé for technical support, Khalid Hamid El Hachimi for expertise in neuropathology, Philippe Ravassard for expertise in embryonic development, Mathias Pietrancosta for comments on the manuscript, and Cell Signaling and David Sabatini for providing Depdc5 antibody. Behavioral studies were performed at the ICM Rodent Behavior Core Facility (Magali Dumont and Doriane Foret), which is supported by the “Fondation pour la Recherche Médicale”, “Institut du Cerveau et de la Moelle épinière” and “Institut Hospitalo-Universitaire”. Imaging was performed at the PICPS platform and ICM imaging platform. S.I. is supported by a fellowship from the Japan Society for the Promotion of Science (JSPS).

Appendix A. Supplementary data

Supplementary data to this article can be found online at http://dx.doi.org/10.1016/j.nbd.2016.02.010.

References

Abdijadid, S., et al., 2015. Basic mechanisms of epileptogenesis in pediatric cortical dysplasia. CNS Neurosci. Ther. 21, 92–103.
Acosta-Jaquez, H.A., et al., 2009. Site-specific mTOR phosphorylation promotes mTORC1-mediated signaling and cell growth. Mol. Cell. Biol. 29, 4308–4324.
Anderl, S., et al., 2011. Therapeutic value of prenatal rapamycin treatment in a mouse brain model of tuberous sclerosis complex. Hum. Mol. Genet. 20, 4597–4604.
Bar-Peled, L., et al., 2013. A tumor suppressor complex with GAP activity for the Rag GTPases that signal amino acid sufficiency to mTORC1. Science 340, 1100–1106.
Bateup, H.S., et al., 2013. Excitatory/inhibitory synaptic imbalance leads to hippocampal hyperexcitability in mouse models of tuberous sclerosis. Neuron 78, 510–522.
Baulac, S., et al., 2015. Familial focal epilepsy with focal cortical dysplasia due to DEPDC5 mutations. Ann. Neurol. 77, 675–683.
Baulac, S., et al., 2012. A rat model for LGI1-related epilepsies. Hum. Mol. Genet. 21, 3546–3557.
Baybis, M., et al., 2004. mTOR cascade activation distinguishes tubers from focal cortical dysplasia. Ann. Neurol. 56, 478–487.

Blumcke, I., et al., 2011. The clinicopathologic spectrum of focal cortical dysplasias: a consensus classification proposed by an ad hoc task force of the ILAE diagnostic methods commission. Epilepsia 52, 158–174.
D'Gama, A.M., et al., 2015. Mammalian target of rapamycin pathway mutations cause hemimegalencephaly and focal cortical dysplasia. Ann. Neurol. 77, 720–725.
Degenetais, E., et al., 2002. Electrophysiological properties of pyramidal neurons in the rat prefrontal cortex: an in vivo intracellular recording study. Cereb. Cortex 12, 1–16.
Dibbens, L.M., et al., 2013. Mutations in DEPDC5 cause familial focal epilepsy with variable foci. Nat. Genet. 45, 546–551.
Dutchak, P.A., et al., 2015. Regulation of hematopoiesis and methionine homeostasis by mTORC1 inhibitor NPRL2. Cell Rep. 12, 371–379.
Efeyan, A., et al., 2014. RagA, but not RagB, is essential for embryonic development and adult mice. Dev. Cell 29, 321–329.
Goto, J., et al., 2011. Regulable neural progenitor-specific Tsc1 loss yields giant cells with organellar dysfunction in a model of tuberous sclerosis complex. Proc. Natl. Acad. Sci. U. S. A. 108, E1070–E1079.
Ishida, S., et al., 2013. Mutations of DEPDC5 cause autosomal dominant focal epilepsies. Nat. Genet. 45, 552–555.
Ishida, S., et al., 2012. Kcna1-mutant rats dominantly display myokymia, neuromyotonia and spontaneous epileptic seizures. Brain Res. 1435, 154–166.
Kobayashi, T., et al., 2001. A germ-line Tsc1 mutation causes tumor development and embryonic lethality that are similar, but not identical to, those caused by Tsc2 mutation in mice. Proc. Natl. Acad. Sci. U. S. A. 98, 8762–8767.
Kowalczyk, M.S., et al., 2012. Nprl3 is required for normal development of the cardiovascular system. Mamm. Genome 23, 404–415.
Lal, D., et al., 2014. DEPDC5 mutations in genetic focal epilepsies of childhood. Ann. Neurol. 75, 788–792.
Laplante, M., Sabatini, D.M., 2012. mTOR signaling in growth control and disease. Cell 149, 274–293.
Lasarge, C.L., Danzer, S.C., 2014. Mechanisms regulating neuronal excitability and seizure development following mTOR pathway hyperactivation. Front. Mol. Neurosci. 7, 18.
Liang, N., et al., 2014. Regulation of YAP by mTOR and autophagy reveals a therapeutic target of tuberous sclerosis complex. J. Exp. Med. 211, 2249–2263.
Lim, K.C., Crino, P.B., 2013. Focal malformations of cortical development: new vistas for molecular pathogenesis. Neuroscience 252, 262–276.
Lozovaya, N., et al., 2014. Selective suppression of excessive GluN2C expression rescues early epilepsy in a tuberous sclerosis murine model. Nat. Commun. 5, 4563.
Ma, A., et al., 2014. Tsc1 deficiency-mediated mTOR hyperactivation in vascular endothelial cells causes angiogenesis defects and embryonic lethality. Hum. Mol. Genet. 23, 693–705.
Mahon, S., Charpier, S., 2012. Bidirectional plasticity of intrinsic excitability controls sensory inputs efficiency in layer 5 barrel cortex neurons in vivo. J Neurosci. 32, 11377–11389.
Martin, C., et al., 2014. A recurrent mutation in DEPDC5 predisposes to focal epilepsies in the French-Canadian population. Clin. Genet. 86, 570–574.
Mashimo, T., et al., 2013. Efficient gene targeting by TAL effector nucleases coinjected with exonucleases in zygotes. Sci Rep. 3, 1253.
Mashimo, T., et al., 2010. A missense mutation of the gene encoding voltage-dependent sodium channel (Nav1.1) confers susceptibility to febrile seizures in rats. J Neurosci. 30, 5744–5753.
Meikle, L., et al., 2008. Response of a neuronal model of tuberous sclerosis to mammalian target of rapamycin (mTOR) inhibitors: effects on mTORC1 and Akt signaling lead to improved survival and function. J Neurosci. 28, 5422–5432.
Meikle, L., et al., 2007. A mouse model of tuberous sclerosis: neuronal loss of Tsc1 causes dysplastic and ectopic neurons, reduced myelination, seizure activity, and limited survival. J Neurosci. 27, 5546–5558.
Miyata, H., et al., 2004. Insulin signaling pathways in cortical dysplasia and TSC-tubers: tissue microarray analysis. Ann. Neurol. 56, 510–519.
Nunez, A., et al., 1993. Electrophysiology of cat association cortical cells in vivo: intrinsic properties and synaptic responses. J. Neurophysiol. 70, 418–430.
Onda, H., et al., 1999. Tsc2(+/−) mice develop tumors in multiple sites that express gelsolin and are influenced by genetic background. J. Clin. Invest. 104, 687–695.
Panchaud, N., et al., 2013. Amino acid deprivation inhibits TORC1 through a GTPase-activating protein complex for the rag family GTPase Gtr1. Sci Signal. 6, ra42.
Paxinos, G.W.,.C., 2005. The Rat Brain in Stereotaxic Coordinates.
Paz, J.T., et al., 2009. Multiple forms of activity-dependent intrinsic plasticity in layer V cortical neurones in vivo. J. Physiol. 587, 3189–3205.
Picard, F., et al., 2014. DEPDC5 mutations in families presenting as autosomal dominant nocturnal frontal lobe epilepsy. Neurology 82, 2101–2106.
Polack, P.O., Charpier, S., 2006. Intracellular activity of cortical and thalamic neurones during high-voltage rhythmic spike discharge in Long–Evans rats in vivo. J. Physiol. 571, 461–476.
Polack, P.O., et al., 2009. Inactivation of the somatosensory cortex prevents paroxysmal oscillations in cortical and related thalamic neurons in a genetic model of absence epilepsy. Cereb. Cortex 19, 2078–2091.
Rennebeck, G., et al., 1998. Loss of function of the tuberous sclerosis 2 tumor suppressor gene results in embryonic lethality characterized by disrupted neuroepithelial growth and development. Proc. Natl. Acad. Sci. U. S. A. 95, 15629–15634.
Ricos, M.G., et al., 2016. Mutations in the mTOR pathway regulators NPRL2 and NPRL3 cause focal epilepsy. Ann. Neurol. 79, 120–131.
Sakuma, T., et al., 2013. Repeating pattern of non-RVD variations in DNA-binding modules enhances TALEN activity. Sci Rep. 3, 3379.
Scerri, T., et al., 2015. Familial cortical dysplasia type IIA caused by a germline mutation in DEPDC5. Ann. Clin. Transl. Neurol. 2, 575–580.
Scheffer, I.E., et al., 2014. Mutations in mammalian target of rapamycin regulator DEPDC5 cause focal epilepsy with brain malformations. Ann. Neurol. 75, 782–787.
Sim, J.C., et al., 2016. Familial cortical dysplasia caused by mutation in the mTOR regulator NPRL3. Ann. Neurol. 79, 132–137.
Tsai, P.T., et al., 2013. Prenatal rapamycin results in early and late behavioral abnormalities in wildtype C57BL/6 mice. Behav. Genet. 43, 51–59.
Way, S.W., et al., 2012. The differential effects of prenatal and/or postnatal rapamycin on neurodevelopmental defects and cognition in a neuroglial mouse model of tuberous sclerosis complex. Hum. Mol. Genet. 21, 3226–3236.
Wiegand, G., et al., 2013. Everolimus in tuberous sclerosis patients with intractable epilepsy: a treatment option? Eur. J. Paediatr. Neurol. 17, 631–638.
Yang, S.B., et al., 2012. Rapamycin ameliorates age-dependent obesity associated with increased mTOR signaling in hypothalamic POMC neurons. Neuron 75, 425–436.